

Radflow: A Recurrent, Aggregated, and Decomposable Model for Networks of Time Series

Alasdair Tran^{1,2}, Alexander Mathews¹, Cheng Soon Ong^{1,2}, Lexing Xie¹

¹ Australian National University ² Data61, CSIRO

{alasdair.tran,alex.mathews,chengsoon.ong,lexing.xie}@anu.edu.au

ABSTRACT

We propose a new model for networks of time series that influence each other. Graph structures among time series are found in diverse domains, such as web traffic influenced by hyperlinks, product sales influenced by recommendation, or urban transport volume influenced by road networks and weather. There has been recent progress in graph modeling and in time series forecasting, respectively, but an expressive and scalable approach for a network of series does not yet exist. We introduce Radflow, a novel model that embodies three key ideas: a recurrent neural network to obtain node embeddings that depend on time, the aggregation of the flow of influence from neighboring nodes with multi-head attention, and the multi-layer decomposition of time series. Radflow naturally takes into account dynamic networks where nodes and edges change over time, and it can be used for prediction and data imputation tasks. On real-world datasets ranging from a few hundred to a few hundred thousand nodes, we observe that Radflow variants are the best performing model across a wide range of settings. The recurrent component in Radflow also outperforms N-BEATS, the state-of-the-art time series model. We show that Radflow can learn different trends and seasonal patterns, that it is robust to missing nodes and edges, and that correlated temporal patterns among network neighbors reflect influence strength. We curate WIKITRAFFIC, the largest dynamic network of time series with 366K nodes and 22M time-dependent links spanning five years. This dataset provides an open benchmark for developing models in this area, with applications that include optimizing resources for the web. More broadly, Radflow has the potential to improve forecasts in correlated time series networks such as the stock market, and impute missing measurements in geographically dispersed networks of natural phenomena.

ACM Reference Format:

Alasdair Tran, Alexander Mathews, Cheng Soon Ong, Lexing Xie. 2021. Radflow: A Recurrent, Aggregated, and Decomposable Model for Networks of Time Series. In *Proceedings of the Web Conference 2021 (WWW '21)*, April 19–23, 2021, Ljubljana, Slovenia. ACM, New York, NY, USA, 12 pages. <https://doi.org/10.1145/3442381.3449945>

KEYWORDS

time series, networks, graphs, sequence models, wikipedia

This paper is published under the Creative Commons Attribution 4.0 International (CC-BY 4.0) license. Authors reserve their rights to disseminate the work on their personal and corporate Web sites with the appropriate attribution.

WWW '21, April 19–23, 2021, Ljubljana, Slovenia

© 2021 IW3C2 (International World Wide Web Conference Committee), published under Creative Commons CC-BY 4.0 License.

ACM ISBN 978-1-4503-8312-7/21/04.

<https://doi.org/10.1145/3442381.3449945>

1 INTRODUCTION

Forecasting time series is a long-standing research problem that is applicable to econometrics, marketing, astronomy, ocean sciences, and other domains. Similarly, networks are the subject of active research with broad relevance to areas such as transportation, internet infrastructure, signaling in biological processes, and online media. In this paper, we are concerned with forecasting among a network of time series with mutual influences. Tools for tackling this problem will help answer questions about complex systems evolving over time in the above application domains and beyond.

In the context of recent progress in end-to-end learning for time series and large networks, there are three prominent challenges. The first is *expressiveness*, i.e. building models to represent richer classes of functions. Recent works in predicting book sales [6] and online video views [38] employed simple aggregation [6] or linear combinations [38] of the last observation of incoming nodes. Recent graph neural networks [8, 14, 35] provide flexible aggregation among network neighbors, but do not readily apply to time series. N-BEATS [21] is the new state-of-the-art model in time series benchmarks, using a stack of neural modules to decompose history; but this architecture does not provide a usable representation for a network of series as the neural modules do not explicitly encode the temporal structure of the data. There are several graph-to-sequence tasks [4, 39] considered in the natural language processing (NLP) domain, but the networks of time series problem, cast in such terminology, is graphs-of-sequences to graphs-of-sequences.

The second challenge is *scale*. Our goal is to model longitudinal (e.g., daily) time series spanning a few years, and large networks in the order of hundreds of thousands of nodes. This requires scalability in the time series component, the graph component, as well as their interactions. The recently proposed T-GCN model [40], for example, nests a graph neural network within a recurrent neural network, which is limited in both space and time complexity that prevents it from scaling to web-scale networks. The networks used in their evaluation contain only a few hundred nodes.

The third is the *dynamic nature of links and nodes in the network*. For example, Wu et al. [38] reported that 50% of online video recommendation links appear in fewer than 5 out of 63 days of observation, and we observe that more than 100K new Wikipedia pages were created over the first half of 2020 alone. Dynamic networks are an active topic of attention for graph neural networks [18, 22, 33], but these existing algorithms are designed for link prediction and node classification, not for time series forecasting.

We propose a novel neural model for networks of time series that tackles all three challenges. We adopt a **Recurrent** structure that affords time-sensitive Aggregations of network flow on top of the **Decomposition** principle of time series; hence the name **Radflow**. It is more expressive than N-BEATS [21] because it can generate

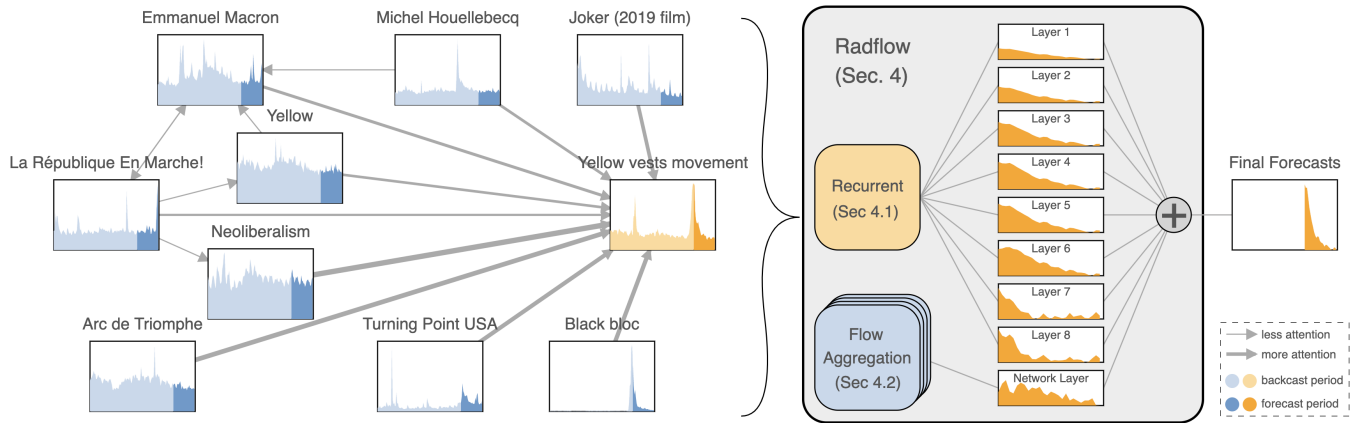


Figure 1: Overview of the Radflow model, centered around the WIKITRAFFIC subgraph of *Yellow vests movement* (a social movement in France since 2018, shown on the left). Each node is a page with a time series of view counts, shown in its individual mini-panel. Edge strengths correspond to average attention scores in the forecast period. The final forecast is produced by summing over the output from eight layers of the recurrent component and the network flow aggregation component (shown on the right). Radflow correctly predicts a sharp drop in traffic volume for *Yellow vests movement* from 3 June 2020 to 30 June 2020, due to information from neighboring nodes such as *Black bloc* and *Turning Point USA*.

node embeddings to handle graph inputs. It is more scalable than T-GCN as it can process hundreds of thousands of nodes via network attention and importance-weighted node sampling. The structure of Radflow allows it to take dynamically changing nodes and edges as inputs, makes it tolerant to missing data, and is suitable for multivariate time series. Moreover, its multi-head attention strategy and layered decompositions provide interpretations over network influences and time.

Radflow is evaluated on four datasets. Two are on urban traffic consisting of several hundred nodes; two are large-scale datasets—VEVO MUSIC containing 61K videos [38] and a newly curated WIKITRAFFIC dataset containing 366K pages and 22M dynamic links. On both VEVO MUSIC and WIKITRAFFIC, Radflow without network information is consistently better than the comparable N-BEATS [21]. Among models with network information, Radflow variants perform the best in both imputation and forecasting tasks. In particular, Radflow outperforms state-of-the-art ARNet [38] by 19% in SMAPE score on VEVO MUSIC. We find that the layers in the recurrent component capture different seasonality and trends, while attention over the network captures the time-varying influence from neighboring nodes. Fig. 1 illustrates the task of predicting 28 days of view counts on *Yellow vests movement*, based on the historical traffic of that page and the traffic of the neighboring pages. Radflow correctly predicts the sharp drop that is observed during the test period.

Our key contributions include:

- (1) Radflow, an end-to-end neural forecasting model for dynamic networks of multivariate time series that is scalable to hundreds of thousands of nodes.
- (2) Interpretable predictions over time series patterns via layered decompositions, and over network neighbors via multi-head attention.
- (3) Consistently outperforming state-of-the-art time series forecasting models and networked series forecasting models in real-world datasets across a diverse set of tasks.

- (4) WIKITRAFFIC, the largest dynamic network of time series, containing multi-dimensional traffic data from 366K Wikipedia pages and 22M dynamic links over five years. The dataset, code, and pretrained models are available on GitHub¹.

2 RELATED WORKS

2.1 Time series modeling

Time series modeling has an extensive literature spanning many fields. Classical approaches [11] include exponential smoothing and autoregressive integrated moving average (ARIMA) models. Exponential smoothing uses exponentially decaying weights of past observations, while extensions can incorporate both trends and seasonality [3, 10, 36]. ARIMA [2] models aim to describe auto-correlations in a time series using a linear combination of past observations and forecasting errors; extensions can also incorporate seasonality. In recent years, neural network approaches have become more popular. Wu et al. [37] used transformers to forecast influenza activities. Zhu and Laptev [42] used a Bayesian neural network to model uncertainty in the forecasting.

Oreshkin et al. [21] were the first to show that a pure neural model without any time series-specific component can outperform existing statistical techniques on the benchmark datasets M3 [16], M4 [17], and TOURISM [1]. Their proposed model, N-BEATS, treats the time series prediction as a non-linear multivariate regression problem that outputs a fixed-length vector as the forecast. N-BEATS' key modeling component is the stacking of layers, each of which takes as input the residual time series calculated by the previous layers. However, N-BEATS only works with one-dimensional time series and does not produce a time series representation vector at each step, making it difficult to be used in settings with dynamic network information. We address both of these shortcomings by adopting the recurrent network structure that produces time series

¹<https://github.com/alsadairtran/radflow>

representations (which we call embeddings) at any time step, while still taking advantage of the residual stacking idea from N-BEATS.

Another type of time series is discrete events happening in continuous time, often described by temporal point processes. Predictive approaches using point processes [19] require the data to contain details of individual events rather than the aggregate statistics that are more common in large-scale web data due to privacy and storage constraints. Point process estimation models are typically quadratic in the number of events, which is too expensive for large-scale data like VEVO MUSIC and WIKITRAFFIC.

2.2 Prediction over networks

Network effects in online services are an active area of research that studies how links between online items determine properties such as visibility, influence, and future behavior. Social networks and information networks are frequently studied in this context. On Twitter, Su et al. [29] showed that the introduction of a new network-based recommender system resulted in a substantial change to the network structure, exacerbating the “rich get richer” phenomenon. On Wikipedia, the link structure has been used to track the evolution of emerging topics [12] and the flow of traffic caused by exogenous events [41]. Zhu et al. [41] showed that when a Wikipedia article gains attention from an exogenous event, it can lead to a substantial rise in attention on downstream hyperlinked articles. Kämpf et al. [12] showed that the evolution of an emerging topic can be tracked and predicted using Wikipedia page views and internal links. The product recommendation network on Amazon has been shown to affect purchasing decisions [20]. Wu et al. [38] showed that the network induced by YouTube’s recommender system leads to a flow of influence between music videos.

One recent approach to model the network effect is to use neural graph networks to generate low-dimensional embeddings of nodes in a graph. Early methods such as node2vec [7] and DeepWalk [24] are transductive, designed mainly to work with a fixed graph. Recent models can be applied to an inductive setting that requires generating embeddings for nodes not seen during training. This is done, for example, by sampling and aggregating node features from the local neighborhood in GraphSage [8]. Various aggregation methods have been proposed including max-pooling [8] and mean-pooling [14]. Veličković et al. [35] proposed Graph Attention Network (GAT) that uses a modified version of the multi-head attention [34] to aggregate the neighborhood. In our proposed architecture, network embedding and aggregation are key components. A variety of network aggregation mechanisms can be used (see Section 4.2 and Section 6). Our suggested aggregation mechanism is similar to GAT, but instead uses the original, and more common, dot-product formulation of the multi-head attention.

2.3 Networks of time series

Being a new area of research, there are few forecasting methods and a limited number of datasets for networks of time series. Early approaches ignore the network structure and instead treat each node as an independent series [25, 30]. Wu et al. [38] incorporated the local network structure into an autoregressive time series model, but the architecture only works with a static graph. Zhao et al. [40] proposed a new Recurrent Neural Network (RNN) cell called

T-GCN that takes into account the structure of a static graph by incorporating a Graph Convolution Network (GCN) component. The bundling of these two components and the lack of neighborhood sampling makes T-GCN too computationally expensive to apply to graphs of more than a few hundred nodes.

A related problem is predicting how edges in networks change, such as those using point processes [32, 33] or two-dimensional attention over graphs and time [27]. We do not tackle this problem; instead we assume that the dynamic graph is observed (such as generated by a recommender system or crowd-sourcing), and the prediction target is a time series on each node rather than the evolving graph itself. Our work is the first forecasting model optimized for large dynamic networks of time series.

3 PROBLEM STATEMENT

Consider the problem of time series forecasting in a graph. The input is a graph $G = (V, E)$, consisting of N nodes denoted $V = \{v^1, v^2, \dots, v^N\}$, and M edges. Each node v^j is associated with a multivariate time series having T observations:

$$v^j = [v_1^j, v_2^j, \dots, v_T^j] \quad (1)$$

where $v_t^j \in \mathbb{R}^D$ is the D -dimensional observation vector of node v^j at time step t . When the time series has only one value per time step (univariate), then $D = 1$. We use $v_{[t:s]}^j$ to denote a subsequence of v^j containing all observations from time t to s , where $t \leq s$:

$$v_{[t:s]}^j = [v_t^j, v_{t+1}^j, \dots, v_{s-1}^j, v_s^j] \quad (2)$$

If node v^i has the potential to directly influence the time series of node v^j at time step t , then we add a directed edge e_t^{ij} from v^i to v^j , and v^i becomes a neighbor of v^j . We define $\mathcal{N}_t(v^j)$ to be the set of neighbors of v^j at times step t . Edges may appear and disappear over time, thus G is a dynamic graph. We can now represent G as an adjacency array $A \in \mathbb{R}^{N \times N \times T}$. For an unweighted directed graph, the entry a_{ijt} in A is 1 if edge e_t^{ij} exists, and 0 otherwise.

We now define the time series forecasting problem as it applies to dynamic graphs. The forecast length F is the number of future time steps for which the model will make predictions, while the backcast length B is the number of past observations available for making such predictions. Suppose we are currently at time $t = 0$. To forecast the time series of node v^j (which we shall call the *ego* node) from time step 1 to F , the forecast model

$$\hat{v}_{[1:F]}^j = \text{ForecastModel}\left(v_{[-B+1:0]}^j, \mathcal{V}^{\mathcal{N}(v^j)}\right) \quad (3)$$

will take two sets of inputs: the B most recent observations of v^j and the information from its neighbors. This leads to two different settings, both of which will be evaluated in Section 7. The first is IMPUTATION, in which we observe the true values of the neighbors at the time of prediction. This amounts to using the ground-truth observations of the neighbors during the forecast period:

$$\mathcal{V}^{\mathcal{N}(v^j)} = \left\{ v'_{[-B+1:F]} \mid v' \in \mathcal{N}(v^j) \right\} \quad (4)$$

This is the setting used by Wu et al. [38] and is most useful when the main goal is to fill in missing data in the time series, or to interpret the influence between nodes. The second setting is FORECAST, where we first use our best pure time series model to predict the future

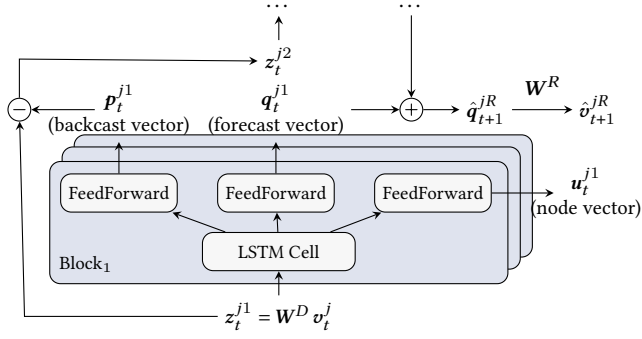


Figure 2: An overview of Radflow’s recurrent block (Section 4.1). Shown here is the first of L blocks at time t , which takes a projected representation z_t^{j1} of the raw observations as input, and produces: the backcast vector p_t^{j1} , the forecast vector q_t^{j1} , and the node vector u_t^{j1} . The backcast vector is subtracted from z_t^{j1} to obtain the (residual) input for the next block. The forecast vector is an additive component for the overall forecast \hat{v}_{t+1}^{jR} in Eq. (15). The node vector will be used when aggregating the neighbors (Section 4.2).

observations of each neighbor. These predictions are then used in the full model to forecast v^j itself.

In both settings, the final output of the model is

$$\hat{v}_{[1,F]}^j = [\hat{v}_1^j, \hat{v}_2^j, \dots, \hat{v}_F^j] \quad (5)$$

corresponding to the forecast values for the next F time steps. Here we use the hat notation to denote the model’s predictions, e.g., \hat{v}_t^j is the forecast time series vector of the ground truth v_t^j .

4 RADFLOW

Radflow consists of two main modules: a recurrent component and a flow aggregation component. The recurrent component models all the time series in the graph independently, while the flow aggregation component additively adjusts the predictions based on the neighboring time series. The forecast \hat{v}_t^j of node v^j at time step t is obtained by summing up the outputs of the two main modules,

$$\hat{v}_t^j = \hat{v}_t^{jR} + \hat{v}_t^{jA} \quad (6)$$

where \hat{v}_t^{jR} is the forecast contribution from the recurrent component and \hat{v}_t^{jA} is the contribution from the aggregation component. Note that \hat{v}_t^{jA} is itself a function of \hat{v}_t^{jR} .

4.1 Recurrent component

We predict time series by breaking them down into L components using stacked recurrent blocks. The recurrent component is also designed to feed into the flow aggregation component which uses the node vectors to aggregate information in a neighborhood. Fig. 2 shows a schematic diagram of the recurrent component.

We first project the historical observations of the time series into a latent space in \mathbb{R}^H , where H is the hidden state size:

$$z_t^{j1} = W^D v_t^j \quad (7)$$

Here $W^D \in \mathbb{R}^{H \times D}$ is a learnable weight matrix. To get an intuitive justification for this projection, consider the special case where $D = 1$ and W^D is the all-ones vector. Then z_t^{j1} would contain H copies of the observation v_t^j . This resembles running an ensemble of H different time series models in parallel.

The recurrent component of our model consists of L blocks. Let $z_t^{j\ell}$ be the input to Block_ℓ for node v^j at step t . In particular, the vector z_t^{j1} computed in Eq. (7) will be used as the input to the first block. Each block will output three vectors—the backcast vector $p_t^{j\ell}$, the forecast vector $q_t^{j\ell}$, and the node vector $u_t^{j\ell}$:

$$(p_t^{j\ell}, q_t^{j\ell}, u_t^{j\ell}) = \text{Block}_\ell(z_t^{j\ell}) \quad (8)$$

with $p_t^{j\ell}, q_t^{j\ell}, u_t^{j\ell} \in \mathbb{R}^H$. Specifically inside each block, we have an LSTM cell followed by feedforward layers. The LSTM cell is first to operate, accepting as input: the time series residual computed by the previous block $z_t^{j\ell} \in \mathbb{R}^H$, the previous time step’s hidden state $h_{t-1}^{j\ell} \in \mathbb{R}^H$, and the cell state $c_{t-1}^{j\ell} \in \mathbb{R}^H$. The LSTM cell produces a hidden output $h_t^{j\ell}$, which is then passed through three different feedforward layers:

$$p_t^{j\ell} = \text{FeedForward}^{P\ell}(h_t^{j\ell}) \quad (9)$$

$$q_t^{j\ell} = \text{FeedForward}^{Q\ell}(h_t^{j\ell}) \quad (10)$$

$$u_t^{j\ell} = \text{FeedForward}^{U\ell}(h_t^{j\ell}) \quad (11)$$

Each of the feedforward layers consists of two linear projections with a GELU activation after the first linear projection:

$$\text{FeedForward}(\mathbf{h}) = W^{FF_2} \text{GELU}(W^{FF_1} \mathbf{h}) \quad (12)$$

The GELU activation function is a stochastic variant of ReLU that has been shown to outperform ReLU in sequence-to-sequence models [9]. It is defined as $\text{GELU}(x) = x \Phi(x)$, where Φ is the standard Gaussian cumulative distribution function.

The first output $p_t^{j\ell}$ is a component of the projected time series captured by Block_ℓ . Subsequent blocks depend on the residual value of the projected time series after removing this component:

$$z_t^{j\ell+1} = z_t^{j\ell} - p_t^{j\ell} \quad (13)$$

The second output $q_t^{j\ell}$ is Block_ℓ ’s contribution to the forecast of the next time step. The final forecast representation of the recurrent component will be the sum of all the blocks

$$\hat{q}_{t+1}^{jR} = \sum_{\ell=1}^L q_t^{j\ell} \quad (14)$$

where $\hat{q}_{t+1}^{jR} \in \mathbb{R}^H$. We then project this into \mathbb{R}^D to get the forecast contribution from the recurrent component, i.e. the first term in Eq. (6):

$$\hat{v}_{t+1}^{jR} = W^R \hat{q}_{t+1}^{jR} \quad (15)$$

4.2 Flow aggregation component

The flow aggregation component models the influence between the time series of neighboring nodes in the network. This component takes as input time-dependent embeddings from the recurrent component of each node in the neighborhood, and produces as output the second term in Eq. (6). Each embedding summarizes the

time series of the corresponding node up to the current time. Let \mathbf{u}_t^j be the embedding of the ego node v^j at time step t , formed by summing the node vectors $\mathbf{u}_t^{j\ell}$ over all L blocks:

$$\mathbf{u}_t^j = \sum_{\ell=1}^L \mathbf{u}_t^{j\ell} \quad (16)$$

In the IMPUTATION setting, the set of embeddings of all neighbors of the ego at time $t+1$ is

$$\mathcal{U}_{t+1}^{\mathbf{v}^j} = \{\mathbf{u}_{t+1}^i \mid i \text{ s.t. } v^i \in \mathcal{N}_{t+1}(v^j)\} \quad (17)$$

while in the FORECAST setting, we simply replace the ground truth \mathbf{u}_{t+1}^i with the forecast $\hat{\mathbf{u}}_{t+1}^i$. We now project the ego's embedding into the query space,

$$\mathbf{u}_t^{Qj} = \mathbf{W}^Q \mathbf{u}_t^j \quad (18)$$

and the neighbors' embeddings into the key and value space,

$$\mathbf{u}_{t+1}^{Ki} = \mathbf{W}^K \mathbf{u}_{t+1}^i \quad \forall i \text{ s.t. } v^i \in \mathcal{N}_{t+1}(v^j) \quad (19)$$

$$\mathbf{u}_{t+1}^{Vi} = \mathbf{W}^V \mathbf{u}_{t+1}^i \quad \forall i \text{ s.t. } v^i \in \mathcal{N}_{t+1}(v^j) \quad (20)$$

The aggregated embedding $\tilde{\mathbf{u}}_{t+1}^j$ is then the weighted sum of the values with a GELU activation,

$$\tilde{\mathbf{u}}_{t+1}^j = \text{GELU}\left(\sum_i \lambda_i \mathbf{u}_{t+1}^{Vi}\right) \quad (21)$$

where the weights λ_i , called *attention scores*, are computed from the dot product between the query and the keys, followed by a softmax. Note that the ego node is not included in the aggregation; instead it is added separately,

$$\hat{\mathbf{u}}_{t+1}^j = \mathbf{W}^E \mathbf{u}_t^j + \mathbf{W}^N \tilde{\mathbf{u}}_{t+1}^j \quad (22)$$

which is then projected down to \mathbb{R}^D ,

$$\hat{\mathbf{v}}_{t+1}^{jA} = \mathbf{W}^A \hat{\mathbf{u}}_{t+1}^j \quad (23)$$

The vector $\hat{\mathbf{v}}_{t+1}^{jA}$ is the forecast contribution from the flow aggregation component, i.e. the second term in Eq. (6).

We call the full model with multi-head attention *Radflow*. Note that the flow aggregation component and the recurrent component are decoupled. Thus we can easily substitute the multi-head attention with another node aggregation method. In particular, if we replace Eq. (21) with a simple arithmetic average of the neighbors,

$$\tilde{\mathbf{u}}_{t+1}^j = \frac{1}{|\mathcal{N}_{t+1}(v^j)|} \sum_i \mathbf{u}_{t+1}^i \quad (24)$$

we would obtain the original formulation of GraphSage [8]. We call the model that uses Eq. (24) instead of Eq. (21) *Radflow-GraphSage*. In addition to adopting Eq. (24), a further simplification is to remove the linear projection in Eq. (22) when adding the ego's embedding with its neighbors'. Let us call this variant *Radflow-MeanPooling*.

4.3 Relationship with existing models

4.3.1 GAT. Our multi-head attention neighborhood aggregation is similar to the Graph Attention Network (GAT) [35]. To compute the attention score in GAT, we first need to concatenate the ego node's embedding with the neighbor's, and then feed the result through a single feedforward network followed by a LeakyReLU. In contrast, we revert back to the original multi-head attention [34]

where we compute the attention scores with a simple dot product. We also add zero attention, in which a node has the option not to attend to any neighbor. We will empirically show in Section 7 that our simpler method outperforms GAT in almost all settings.

4.3.2 N-BEATS. The process of feeding residuals of time series into deep network layers is inspired by N-BEATS. However, N-BEATS takes residuals from the raw scalar observations, whereas our approach calculates the residuals from the vector-valued projections of the time series, as shown in Eq. (7). Moreover, N-BEATS is not easily adapted to the dynamic graph setting since it does not produce embeddings that depend on time. N-BEATS treats the forecasting task as a multivariate regression problem, where every step can see every other step in the history. This allows us to obtain an embedding for the whole series but not for an individual step. In our proposed architecture, the node vector $\mathbf{u}_t^{j\ell}$ is used to construct the time-dependent embedding of each step, as shown in Eq. (16).

4.3.3 Transformers. In the last few years, transformers [34] have become the sequence model of choice in the NLP domain. Despite their success in NLP tasks, little progress has been made with time series forecasting. Most recently, Wu et al. [37] designed a transformer to forecast flu cases, but their model provides only marginal improvement over the LSTM baseline. Our preliminary investigation indicated that LSTMs perform better than transformers in the time series setting. We hypothesize that the strict temporal ordering of the LSTM can encode time series more naturally; while text, which often has a latent tree structure, is more naturally encoded by the transformer with its attention mechanism and position encodings.

4.3.4 Non-neural aggregation. The most relevant non-neural aggregation approach is ARNet [38], a forecasting model for scalar-valued time series in which the prediction is computed as:

$$\hat{v}_t^j = \sum_{k=1}^p \alpha_k^j v_{t-k}^j + \sum_{v^i \in \mathcal{N}(v^j)} \beta^{ij} v_t^i \quad (25)$$

where the first term is an autoregressive model of order $p = 7$ (days) and the second term models the network effect. The learnable parameters β^{ij} can be interpreted as the edge weight that controls the proportion of views propagating from node i to node j . Although ARNet is simple with a straightforward interpretation, the model assumes that the network is static. Furthermore Wu et al. [38] only evaluated on the IMPUTATION setting and not on the FORECAST setting where the future observations are unknown. We will show in Section 7 that the added complexity of Radflow allows it to both incorporate dynamic graphs and function in the FORECAST setting.

4.3.5 Neural aggregation. The closest model to ours is T-GCN [40], where a modified GRU cell does a graph convolution before computing the update and reset gates. Unlike Radflow which has been implemented to fetch subgraphs from disk and only compute the network information once after the final LSTM layer, T-GCN requires the entire network to be in memory and aggregates the network at every time step in every layer. Therefore, T-GCN does not scale to larger datasets due to both space and time complexity. Our proposed architecture, on the other hand, can easily handle dynamic networks of hundreds of thousands of nodes.

Table 1: Key statistics on two snapshots (the first and last day) of VEVO MUSIC and WIKITRAFFIC.

	VEVOMUSIC		WIKITRAFFIC	
	1 Sep 18	2 Nov 18	1 Jul 15	30 Jun 20
Number of nodes	60,663	60,664	329,255	366,145
Number of edges	1,189,460	1,192,478	12,869,374	17,417,749
Nodes with in-edges	56,852	56,672	303,440	356,120
Mean in-degree	21	21	42	49
Median in-degree	10	10	14	17
Nodes with out-edges	60,553	60,545	319,426	362,148
Mean out-degree	20	20	40	48
Median out-degree	19	19	26	31
Diameter	32	27	15	22
Average path length	8.4	8.3	4.1	4.0
Clustering coefficient	0.17	0.15	0.014	0.015

5 DYNAMIC NETWORKS OF TIME SERIES

The empirical validation of Radflow is carried out on two small static networks—LOS-LOOP and SZ-TAXI [40]; and two large-scale dynamic networks—VEVOMUSIC [38] and WIKITRAFFIC. Out of these, WIKITRAFFIC is a new dataset that we have collected and it is the largest dynamic network of time series to date. This section describes each dataset in detail.

5.1 LOS-LOOP and SZ-TAXI

LOS-LOOP and SZ-TAXI [40] contain time series of traffic speeds and road network information. LOS-LOOP is a network of 207 sensors, measuring traffic speeds at 5-minute intervals from 1 March to 7 March 2012. There is an edge between two sensors if they are close to each other. SZ-TAXI is a network of 156 roads in the Luohu District in Shenzhen, containing 15-minute interval traffic speeds from 1 January to 31 January 2015. If two roads are connected, an edge is formed between them. Both are static networks, with LOS-LOOP containing 2,833 edges and SZ-TAXI containing 532. We use these datasets to compare Radflow against T-GCN [40].

5.2 VEVOMUSIC

VEVOMUSIC [38] is a YouTube video network containing 60,740 music videos from 4,435 unique artists. Each node in the network corresponds to a video and is associated with a time series of daily view counts collected over the course of 63 days from 1 September 2018 to 2 November 2018. A directed edge from video u to video v is present on day t if v appears on u 's list of recommendations on day t .

To ensure a fair comparison, we use the chronological train-test split by Wu et al. [38], in which we train on the first 49 days, validate on the next 7 days, and test on the final 7 days. We also follow the original setup which computes evaluation metrics on the 13,710 nodes with at least one incoming edge. This makes the differences between network and non-network models more apparent.

5.3 WIKITRAFFIC

We collected the new WIKITRAFFIC network dataset which contains 366K nodes with 22 million unique page pairs that have an edge on

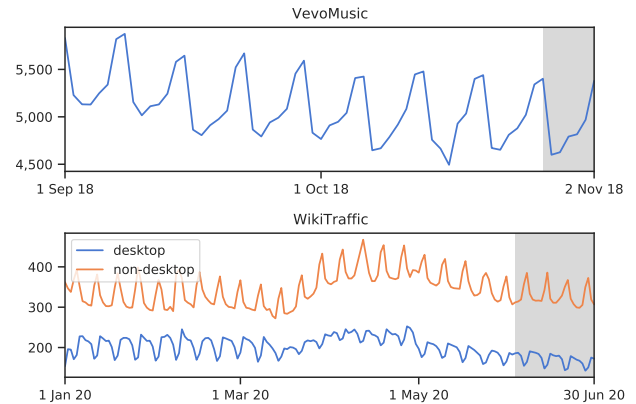


Figure 3: Ground-truth time series averaged across all samples in VEVOMUSIC (top) and WIKITRAFFIC (bottom). Shaded areas correspond to the test period. Strong weekly seasonality can be observed in both datasets.

at least one day over a five-year period. On any given day, we have up to 17 million links, as shown in Table 1. WIKITRAFFIC is similar to VEVOMUSIC in that they both exhibit a strong weekly seasonality (Fig. 3). They both have dynamic links, although WIKITRAFFIC links are more stable overall (Fig. 4).

The data collection starts with the raw dump of the English Wikipedia² containing the full revision history of 17 million articles. From this we collect daily view counts from 1 July 2015 to 30 June 2020. We then remove articles with less than 100 daily average views in the final 140 days. This leaves us with 366,802 pages. The view counts are split into two categories: views from desktop users and from non-desktop users. We set the final 28 days to be the test period, the 28 days before that to be the validation period, and the remaining days for training. Forecasting 28 days in advance allows us to test the robustness of the model when predicting a substantial time into the future.

Furthermore, since WIKITRAFFIC is an order of magnitude larger than other networked time series datasets, we can set aside nodes to be used only during testing. Thus the train-test split is divided both by time and by node, providing a stronger test of a model's ability to generalize. To be useful for evaluating network-based forecasting models, the test set should form its own network, so we choose nodes that are connected. We start with four seed categories: *Programming Languages*, *Star Wars*, *Global Warming*, and *Global Health*, each with many subcategories. Starting with each seed category, we collect all pages in that category and all subcategories within four levels. This provides 2,434 pages for our test set. Finally we consider two versions of the dataset—a univariate version where we predict the total view count of a page, and a bivariate version where we predict the desktop and non-desktop traffic separately.

Prior to our work, Google created a dataset containing two years of traffic from 145K randomly sampled pages in Wikipedia for a Kaggle competition³. However this dataset contains no network

²<https://dumps.wikimedia.org>

³<https://www.kaggle.com/c/web-traffic-time-series-forecasting/data>

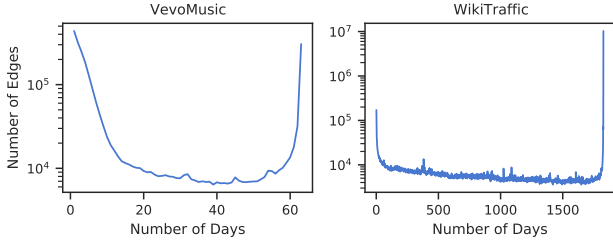


Figure 4: The distribution of link durations. In VEVO MUSIC most links are short-lived (50% appear fewer than five days), likely due to YouTube diversifying its recommendations. In contrast, links in WIKITRAFFIC are more stable, with half persisting throughout the entire five years.

information and includes low-traffic pages which are noisy. Rozemberczki et al. [26] curated a small hyperlink Wikipedia network on specialized topics (chameleons, crocodiles, and squirrels) with only monthly view counts. Consonni et al. [5] introduced WikiLinkGraphs containing all dynamic links from 2001 to 2018, but they did not collect traffic information. In contrast, our WIKITRAFFIC is the largest dynamic network of time series, enabling detailed studies of information flow and user interests on a large scale.

6 EVALUATION SETTINGS

Evaluation is done by predicting view counts of the final 7 days on VEVO MUSIC and the final 28 days on WIKITRAFFIC. For LOS-LOOP and SZ-TAXI, we predict the speeds in the final hour (the final 12 steps in LOS-LOOP and the final 4 steps in SZ-TAXI). As stated in Section 3, we consider both the FORECAST and IMPUTATION settings for the large datasets. On VEVO MUSIC, we evaluate on two different networks: the full dynamic network which we call VEVO MUSIC (dynamic), and the static network which we call VEVO MUSIC (static). To construct the static version, Wu et al. [38] used a majority smoothing method to remove edges that occur only briefly and made the remaining edges persistent in all time steps. Their best model ARNet was only evaluated on this static network in the IMPUTATION setting. On WIKITRAFFIC, we consider two networks: one is a network of univariate time series of view counts, while the other is a network of bivariate time series where desktop and non-desktop traffic are split.

Following prior forecasting work [16, 17], our main evaluation metric will be the Symmetric Mean Absolute Percentage Error for forecast horizon F :

$$\text{SMAPE-}F = \frac{100}{\mathcal{T}FD} \sum_{j=1}^{\mathcal{T}} \sum_{t=1}^F \sum_{d=1}^D \frac{|v_{td}^j - \hat{v}_{td}^j|}{\frac{1}{2} (|v_{td}^j| + |\hat{v}_{td}^j|)} \quad (26)$$

where \mathcal{T} is the number of samples in the test set, F is the forecast horizon, D is the dimension of the time series, and \hat{v}_{td}^j is the forecast value of the ground truth v_{td}^j . SMAPE is interpretable with an upper bound of 200 and a lower bound of 0. It is scale-independent, ensuring that prediction errors will be considered relative to the magnitude of the sequence. This is important because it prevents nodes with a large number of views from dominating the evaluation

measure. A lower SMAPE corresponds to a better fit, with it being 0 if and only if the prediction matches the ground truth perfectly. For the two small networks of univariate time series, LOS-LOOP and SZ-TAXI, we additionally report the Root Mean Square Error,

$$\text{RMSE-}F = \sqrt{\frac{1}{\mathcal{T}F} \sum_{j=1}^{\mathcal{T}} \sum_{t=1}^F (v_t^j - \hat{v}_t^j)^2} \quad (27)$$

and the Mean Absolute Error,

$$\text{MAE-}F = \frac{1}{\mathcal{T}F} \sum_{j=1}^{\mathcal{T}} \sum_{t=1}^F |v_t^j - \hat{v}_t^j| \quad (28)$$

similar to what was done in the T-GCN paper [40].

6.1 Model variants

We compare 8 time series baselines, 7 variants of networked time series, and 7 more variants of Radflow in an ablation study. Results of the following 8 time series baselines are in Table 3 and Table 4.

- (1) **Copying Previous Step:** We use the final observation before the test period as the prediction. This is the final day in VEVO MUSIC and WIKITRAFFIC, the final 5 minutes in LOS-LOOP, and the final 15 minutes in SZ-TAXI.
- (2) **Copying Previous Week:** Since we observe weekly seasonality in both VEVO MUSIC and WIKITRAFFIC (see Fig. 3), a stronger baseline is to copy observations in the final week just before the test period and use them as the predictions.
- (3) **AR:** The autoregressive (AR) model used by Wu et al. [38] for the static VEVO MUSIC network.
- (4) **Seasonal ARIMA:** We train an ARIMA(p, d, q)(P, D, Q) m model separately for each time series, where p, d, q, P, D, Q are the AR, difference, MA, seasonal AR, seasonal difference, and seasonal MA terms, respectively. These are learned automatically using the `pyrardima` package. The number of periods in a season m is set to 7 days for VEVO MUSIC and WIKITRAFFIC.
- (5) **Individual LSTMs:** The LSTM baseline used by Wu et al. [38]. It is trained separately for each time series, with no weight sharing across network nodes.
- (6) **LSTM:** The standard LSTM model with weight sharing. Unlike variant (4), this method uses only one set of LSTM weights for the entire dataset.
- (7) **N-BEATS:** The neural regression with residual stacking from Oreshkin et al. [21]. The implementation consists of eight stacks, each containing one generic block. A generic block internally uses four fully-connected layers, followed by a fork into the forecast and backcast space. For bivariate WIKITRAFFIC, we train two separate N-BEATS models.
- (8) **Radflow-NoNetwork:** Radflow with only the recurrent component, i.e. first term \hat{v}_t^{jR} in Eq. (6). It does not take any contribution from the network.

Results for the forecasting models which use the network structure are presented in Table 4 and 5.

- (9) **T-GCN:** The model proposed by Zhao et al. [40] that uses a modified GRU cell to aggregate nodes. Since T-GCN is not scalable to larger datasets (see Section 4.3), we only compare Radflow against T-GCN on LOS-LOOP and SZ-TAXI [40].

Table 2: Hyperparameters of Radflow-NoNetwork (8) and Radflow (15) on WIKITRAFFIC (univariate). We calibrate the hidden size to ensure that the number of parameters of all models are within 5% of each other. See the Appendix [31] for the hyperparameters of other model variants.

	0 Hops	1 Hop	2 Hops
Number of parameters	1,589,762	1,608,464	1,576,52
LSTM hidden size	128	116	112
Feedforward hidden size	128	116	112
Number of LSTM layers (L)	8	8	8
Dropout probability	0.1	0.1	0.1
Number of attention heads	-	4	4
Backcast (seed) length	112	112	112
Forecast length	28	28	28

- (10) **ARNet**: The state-of-the-art model [38] for the VEVO MUSIC (static) dataset in the IMPUTATION setting (see Section 4.3.4).
- (11) **LSTM-MeanPooling**: The same architecture as (6) but with mean-pooling node aggregation, using the hidden output of the final LSTM layer as a node’s representation.
- (12–15) **Radflow**: Variants of our proposed architecture with different network aggregation techniques: a simple mean (12), GraphSage (13), Graph Attention Network (14), and our full Radflow model with multi-head attention (15). Table 2 outlines the hyperparameters used in the full model.
- Finally we conduct an ablation study to test the key components of our architecture (Table 6). Starting with the best model (15), we substitute one component with an alternative:
- (16–20) **Radflow with other node embeddings**: As shown in Section 4, the LSTM cell contains a hidden state \mathbf{h} which is used to produce three vectors, \mathbf{p} , \mathbf{q} , and \mathbf{u} . Instead of having a separate output \mathbf{u} to represent a node, we could alternatively reuse the cell’s hidden state \mathbf{h} (16), the backcast representation \mathbf{p} (17), or the forecast representation \mathbf{q} (18). We could also concatenate different representations, such as $[\mathbf{h}; \mathbf{p}]$ (19) or $[\mathbf{h}; \mathbf{p}; \mathbf{q}]$ (20).
- (21) **Radflow with no final projection**: We ignore the linear projection in Eq. (22) and add the ego node’s embedding to its neighbors’ directly.
- (22) **Radflow with one attention head**: This final variant tests the effect of having only one attention head instead of the default four in the full model.

6.2 Data preprocessing and training details

Web-scale time series observations often vary greatly in scale. An unpopular page might get zero views, while a popular page might receive millions of visits daily. To ensure similar scaling, both the inputs and outputs of our models are log-transformed time series. Outputs are exponentiated before computing SMAPE, RMSE, and MAE. Missing views are imputed by propagating the last valid observation forward. We do not apply any other preprocessing techniques to the time series, such as trend or seasonality removal.

Table 2 shows key hyperparameters of Radflow. We trained all models on the SMAPE objective using the Adam optimizer [13] with

Table 3: Performance of time series models with no network information. We report mean SMAPE-7 on VEVO MUSIC (22 Oct 18 – 2 Nov 18) and mean SMAPE-28 on WIKITRAFFIC (3 Jun 20 – 30 Jun 20). Rows are numbered according to Sec 6.1. See the Appendix [31] for statistical significance tests.

	VEVO MUSIC	WIKITRAFFIC (univariate)	WIKITRAFFIC (bivariate)
(1) Copying Previous Step	14.0	22.5	26.8
(2) Copying Previous Week	10.3	21.0	25.4
(3) AR [38]	10.2	-	-
(4) Seasonal ARIMA	9.67	19.6	22.8
(5) Individual LSTMs [38]	9.99	-	-
(6) LSTM	8.68	16.6	20.4
(7) N-BEATS	8.64	16.6	20.3
(8) Radflow-NoNetwork	8.42	16.1	19.4

Table 4: FORECAST performance on the static traffic networks. On Los-LOOP, we report mean SMAPE-12, RMSE-12, and MAE-12. On SZ-TAXI, we report mean SMAPE-4, RMSE-4, and MAE-4.

	Los-LOOP			SZ-TAXI		
	SMAPE	RMSE	MAE	SMAPE	RMSE	MAE
(1) Copying Previous Step	3.92	3.40	2.39	45.8	4.32	2.81
(8) Radflow-NoNetwork	3.60	3.23	2.18	80.2	3.99	3.06
(9) T-GCN [40]	3.97	3.42	2.41	80.5	6.27	3.52
(15) Radflow	3.50	3.11	2.11	77.5	3.36	2.51

$\beta_1 = 0.9$, $\beta_2 = 0.999$, $\epsilon = 10^{-8}$. We set the weight decay factor to 10^{-4} and decouple it from the learning rate [15]. We warm up the learning rate to 10^{-4} in the first 5,000 steps and then linearly decay it afterward for 10 epochs, each of which consists of 10,000 steps. We clip the gradient norm at 0.1. All our models are implemented in Pytorch [23]. For a fair comparison, we fix the number of layers of all variants to eight and ensure that size of all variants are within 5% of each other.

6.3 Computational costs

6.3.1 Training time. VEVO MUSIC experiments were trained on a Titan V GPU and WIKITRAFFIC experiments were trained on a Titan RTX GPU. The Titan RTX has twice the memory of the Titan V and is needed to train the two-hop Radflow on WIKITRAFFIC. All pure time series models converge very quickly, taking no more than three hours to train. Models with one-hop aggregation take up to 17 hours to train, while models with two-hop aggregation can take up to two days. We pick the model from the epoch with the lowest SMAPE score on the validation set as our best model.

6.3.2 Efficient computation of graphs. Unlike previous approaches such as T-GCN, our models do not require the whole graph to be in memory during training. Instead we store the graph in the HDF5 format and only load one batch at a time directly from disk.

6.3.3 Neighborhood sampling. To keep the computation tractable, we devise an importance-based neighborhood sampling technique. Instead of the common uniform sampling that was, for example,

Table 5: Performance of models with network information. We report mean SMAPE-7 on VEVO MUSIC (22 Oct 18 – 2 Nov 18) and mean SMAPE-28 on WIKITRAFFIC (3 Jun 20 – 30 Jun 20). Rows are numbered according to Sec 6.1. Bold numbers indicate the best model(s) within a column. Refer to the Appendix [31] for the p-values from the dependent t-test for paired samples between models with similar performance.

	VEVO MUSIC (static)				VEVO MUSIC (dynamic)				WIKITRAFFIC (univariate)				WIKITRAFFIC (bivariate)			
	Forecast		Imputation		Forecast		Imputation		Forecast		Imputation		Forecast		Imputation	
	1H	2H	1H	2H	1H	2H	1H	2H	1H	2H	1H	2H	1H	2H	1H	2H
(10) ARNet [38]	-	-	9.02	-	-	-	-	-	-	-	-	-	-	-	-	-
(11) LSTM-MeanPooling	8.60	8.67	8.14	8.13	8.80	9.03	7.91	7.90	16.8	16.7	15.5	15.2	20.2	19.9	19.2	18.9
(12) Radflow-MeanPooling	8.34	8.44	7.82	7.81	8.42	8.32	7.74	7.61	16.5	16.5	15.1	15.1	19.8	20.2	18.5	18.6
(13) Radflow-GraphSage	8.39	8.37	7.78	7.64	8.43	8.46	7.46	7.27	15.9	16.7	14.7	15.0	19.3	19.9	18.2	18.4
(14) Radflow-GAT	8.52	8.50	7.88	7.74	8.43	8.39	7.44	7.28	16.2	16.0	15.0	15.2	19.5	19.7	18.3	18.6
(15) Radflow	8.33	8.39	7.67	7.63	8.37	8.45	7.32	7.27	16.2	16.0	14.5	14.8	19.9	19.6	18.3	18.5

used by Hamilton et al. [8], we propose a two-stage approach to

select neighbors. First we assign each neighbor a score $\frac{\sum_d v_{td}^j}{\text{outdegree}(\sigma_t^j)+1}$. This score is the total view count of the neighbor at time step t , normalized by the outdegree of the neighbor at that time. A self-loop is added to avoid division by zero. Intuitively, a neighbor with a larger number of views will have a greater influence, but the influence will be more diffuse if that neighbor has many outlinks. Using these scores, we remove neighbors in the bottom 10th percentile in the neighborhood of each ego node, which reduces noise induced by aggregation.

In the second stage, we sample four neighbors during training with probability proportional to the number of time steps that the neighbor appears in the backcast period. During evaluation, we find using all nodes to be computationally infeasible due to the large data size. Thus for each ego node, we choose only the 16 most frequently appearing neighbors in the one-hop setting and the top eight in the two-hop setting.

7 RESULTS

We first discuss prediction performances of different model variants (Sections 7.1 and 7.2, Tables 3 to 6). When applicable, we report in parentheses the p-value (denoted as p) from the dependent t-test for paired samples. All differences discussed in this section are statistically significant. For more detailed significance tests, see the Appendix [31]. We then present a visual interpretation of different layers in the recurrent component (Section 7.3), followed by insights provided by the network aggregation component (Section 7.4). Finally, we present two preliminary studies on the potential applications of models like Radflow: the robustness of predictions when the network is not fully observed (Section 7.5.1), and the relationship between traffic surges on nodes and their attention scores (Section 7.5.2).

7.1 Forecasting and imputation performance

7.1.1 FORECASTING without networks. Table 3 summarizes the comparison between Radflow-NoNetwork and the corresponding time series forecasting baselines (1–7). The LSTM variant (6) outperforms both AR (3) and Seasonal ARIMA (4), showing the robust

Table 6: Ablation study on the key components of Radflow on one-hop VEVO MUSIC networks. See Section 7.2.

	VEVO MUSIC (static)	VEVO MUSIC (dynamic)
(15) Radflow	7.67	7.32
(16) Radflow (\mathbf{h} as embeddings)	7.78	7.51
(17) Radflow (\mathbf{p} as embeddings)	7.77	7.49
(18) Radflow (\mathbf{q} as embeddings)	7.84	7.35
(19) Radflow ($[\mathbf{h}; \mathbf{p}]$ as embeddings)	7.75	7.39
(20) Radflow ($[\mathbf{h}; \mathbf{p}; \mathbf{q}]$ as embeddings)	7.76	7.38
(21) Radflow (no final projection)	7.80	7.33
(22) Radflow (one attention head)	7.77	7.43

performance of flexible neural models. Furthermore, it also outperforms models trained on individual time series (3, 4, 5), highlighting the advantage of using large amounts of training data. N-BEATS (7) outperforms LSTM (6) by a small margin of 0.04 SMAPE ($p = 6e-3$) on VEVO MUSIC, while Radflow-NoNetwork outperforms all other baselines, showing promises in combining the recurrent structure with the residual stacking idea in our architecture. Additionally, Radflow-NoNetwork outperforms ARNet (10), the state-of-the-art for VEVO MUSIC that uses network information (Table 5), indicating that having the right model outweighs having more information for this task.

7.1.2 FORECASTING with networks. Tables 4 and 5 summarize performances of models (9–15) on the four networked time series datasets. Our full model (15) outperforms T-GCN in LOS-LOOP by a non-trivial margin on all metrics. SZ-TAXI is more noisy and no model is able to beat the SMAPE from copying the previous step. This is because SZ-TAXI contains many consecutive zero measurements, which the copying baseline is able to take advantage of. On non-zero test measurements, Radflow is able to outperform all other variants. See the Appendix [31] for these results.

Across all eight FORECASTING settings on VEVO MUSIC and WIKITRAFFIC, the top-performing models are all Radflow variants. Compared to Radflow-NoNetwork (8), incorporating one-hop neighbors improves the SMAPE score on VEVO MUSIC from 8.42 to 8.33 ($p = 2e-33$). On WIKITRAFFIC (univariate), using one-hop GraphSage (13) improves SMAPE from 16.1 to 15.9 ($p = 2e-21$). This

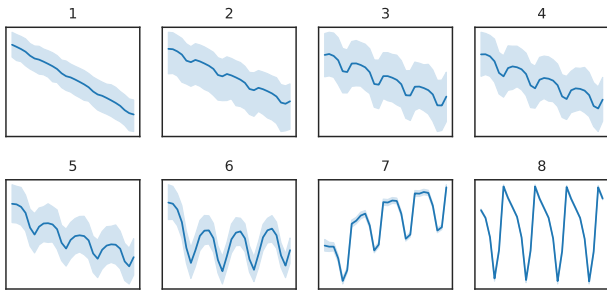


Figure 5: Average prediction over all test pages from each layer of Radflow-NoNetwork on the 28-day test period of WIKITRAFFIC. The light shade corresponds to the 95% confidence interval. Different layers capture different seasonal and trend patterns. See Section 7.3.

confirms the recently reported network effects in the YouTube and Wikipedia traffic [38, 41]. Note that WIKITRAFFIC is much larger and more diverse, making consistent improvements harder, hence the smaller effect size compared to VEVO MUSIC.

Finally, compared to the smoothed static network, using the dynamic network in VEVO MUSIC only improves the performance for some model variants. This is because the static graph was constructed from the smoothing of edges (i.e. uncommon edges were removed), which reduces noise in the absence of ground-truth views from the neighbors. More generally, although Radflow is designed to handle dynamic graphs, it is impossible to know a priori whether dynamic edges will improve the prediction performance in a given data domain.

7.1.3 IMPUTATION. Having ground-truth observations of neighboring nodes during the forecast period leads to substantially better SMAPE scores for all models. Models that perform well in the FORECAST setting also perform well in the IMPUTATION setting, with Radflow (15) achieving the highest SMAPE in six of the eight IMPUTATION settings. The performance gain going from one hop to two hops is more evident in the IMPUTATION setting. For example, there is a boost from 7.67 to 7.63 ($p = 1e-8$) on the static VEVO MUSIC, and from 7.32 to 7.27 ($p = 3e-14$) on the dynamic VEVO MUSIC. Compared to the previous state-of-the-art ARNet [38], our best model achieves a SMAPE score that is 19% better (from 9.02 to 7.27).

On WIKITRAFFIC, using two-hop neighbors uniformly lowers the performance, while the training time more than doubles. Compared to VEVO MUSIC, each Wikipedia page has many more links, most of which would be ignored by the reader. The network effect in WIKITRAFFIC is thus weaker than VEVO MUSIC (see Fig. 6), leading to more noise being introduced in the two-hop setting.

7.2 Radflow components

Among the variants with attention, the weighted multi-head attention of Radflow yields the best performance in 10 out of 16 tasks across FORECAST and IMPUTATION, while GraphSage, which puts an equal weight on all neighbors, is the second best (best in 6 out of 16 tasks). This indicates that simpler attention mechanisms

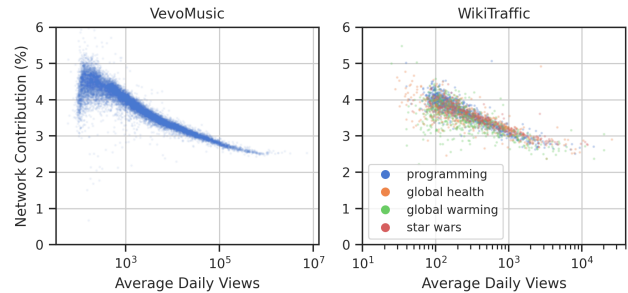


Figure 6: The contribution from the network on the final forecasts. The network component of less popular nodes is larger. For nodes with similar daily view counts, VEVO MUSIC (left) exhibits a stronger network effect than WIKITRAFFIC (right). See Section 7.4.

(inner-product attention in Radflow and node averaging in Radflow-GraphSage) are preferred over more complex ones (Radflow-GAT), but it should not be too simple (Radflow-MeanPooling).

Table 6 presents an ablation study that tests other key components in Radflow. Overall, we find that having more than one attention head helps (15 vs 22), so does a linear projection before node aggregation (15 vs 21). It is also preferable to have a separate projection on the output of the LSTM cell to obtain the node embeddings \mathbf{u} , than to re-use the hidden state \mathbf{h} , the backcast representation \mathbf{p} , or the forecast representation \mathbf{q} (15 vs 16–20). All differences are statistically significant.

7.3 Layered decomposition of time series

The recurrent component of Radflow is decomposable into $L = 8$ layers, via Eqs. (14) and (15). Fig. 5 shows the layer-wise contribution to the forecast from Radflow-NoNetwork. The results are averaged over all 2,434 test pages in WIKITRAFFIC over the 28-day test period, and re-scaled to the same range for readability. We observe that component 8 encodes strong weekly seasonality that is consistent across all test pages (with a small confidence interval). Components 1–5 encode varying levels of a decreasing trend, whereas component 7 encodes an increasing trend. Overall, weekly seasonality is visible in all components except the first, confirming the common intuition that representations learned via neural networks are often over-complete.

7.4 Quantifying effects of the network

7.4.1 Network contribution. Radflow can identify settings where the network information becomes important for the final predictions. Fig. 6 shows the contribution to the final forecast made by the network component (the second term of Eq. (6)). In both VEVO MUSIC and WIKITRAFFIC, there is an approximately inverse linear relationship between the network contribution and the log of average daily views, indicating that forecasts of less popular nodes rely more heavily on the network. For nodes with a similar number of daily views (take, for example, 10^3 views per day), VEVO MUSIC exhibits a stronger network effect (~4%) than WIKITRAFFIC (~3%), indicating that user behaviors on YouTube recommender

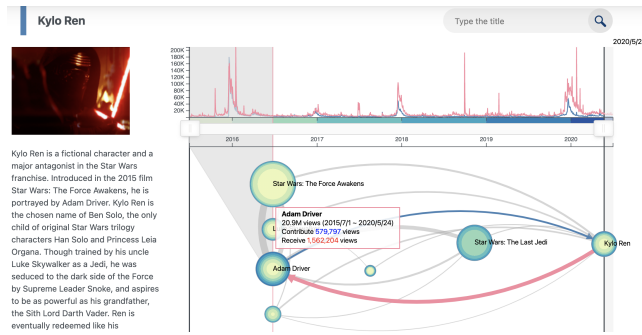


Figure 7: An interactive web app [28] for attention flow, available at <https://attentionflow.ml>. Shown here is the subgraph for the Wikipedia page *Kylo Ren*, a character in *Star Wars* played by *Adam Driver*. The thickness of an edge is determined by the product between the attention score and the traffic volume of the source node. See Section 7.4.2.

links and Wikipedia hyperlinks are different, warranting further investigation (e.g., with user-level data).

7.4.2 Visualising attention flow. The attention scores in Radflow capture some information about the flow of traffic. In particular, we observe that the model pays more attention to a neighboring node on days that have a spike in traffic (see the Appendix [31] for a specific example). This motivates us to visualize the attention flow among WIKITRAFFIC nodes in an interactive web app [28]. In this visualization, nodes are represented in a graph (bottom panel) and as time series (top panel). Edge weights are attention scores from Radflow multiplied by the traffic on the source node.

Fig. 7 is a screenshot for the subgraph centered around the Wikipedia page of *Kylo Ren*, a character in the *Star Wars* series played by the actor *Adam Driver*. From the figure, we observe that the time series of the two nodes (*Kylo Ren* in blue, *Adam Driver* in pink) have synchronized spikes at the same time as the release of major *Star Wars* movies. Furthermore, there appears to be more traffic flowing from *Kylo Ren* to *Adam Driver* than the other way, indicated by the thickness of the edges.

7.5 What if ...

7.5.1 Data is missing? We consider the robustness of Radflow to missing data. This setting is relevant when collecting and observing data from all nodes is very costly (e.g., sites spread out over large geographical areas) or when nodes are simply unavailable (e.g., sites whose data are proprietary). To this end, Fig. 8 shows our evaluation of Radflow on the IMPUTATION task for VEVO MUSIC with a percentage of time series values (left pane) or edges (right pane) deleted at random. As more nodes become missing, the performance of Radflow decays at a much slower rate than Radflow-NoNetwork. This indicates that Radflow is effective in imputing and mitigating missing values from other neighbors. Similarly, Radflow is relatively robust to missing edges. With 40% of edges missing, the performance of the two-hop model only drops by 1% in SMAPE. Even with 80% of edges missing, Radflow is still substantially better than Radflow-NoNetwork.

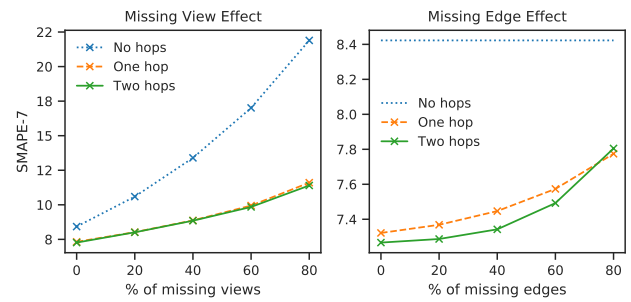


Figure 8: The effect of missing view counts (left) and missing edges (right) on VEVO MUSIC using Radflow. As we delete more data, Radflow’s performance degrades at a much slower rate than Radflow-NoNetwork (in blue). See Section 7.5.1.

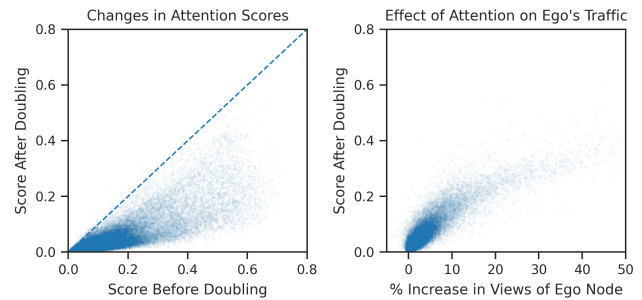


Figure 9: The effect of doubling a neighbor’s view count during the forecast period. Left: scatter plot of attention scores before (x-axis) and after (y-axis) doubling. Right: Scatter plot of the relative increase of the ego node’s views (x-axis) and attention scores after doubling (y-axis). Attention scores decrease as a neighbor becomes more popular (left). A higher attention corresponds to a larger flow of traffic from the neighbor to the ego node (right). See Section 7.5.2.

7.5.2 Node traffic doubles? In addition to the example of an actual traffic spike in Fig. 1, we further perform an evaluation to visualize the effects of hypothetical sudden changes in node traffic. This scenario is useful for planning resources such as edge network caching for mobile videos, or for estimating economic demands associated with nodes such as advertising.

For each test node in the IMPUTATION task on WIKITRAFFIC, we pick one neighbor and double its views on one forecasting day. Fig. 9 (left) shows that as a page becomes more popular, the attention on it uniformly decreases, indicating that attention tends to dampen node traffic spikes instead of amplifying them. More evidently, we can see from Fig. 9 (right) that a higher attention score is *positively correlated with a large effect on the ego node’s traffic*. This indicates that despite the non-linear relationship between attention scores and network component in Section 4, one could qualitatively infer the traffic flow from one page to another using attention scores.

8 CONCLUSION

We propose Radflow, an end-to-end model for forecasting a network of time series. It is expressive with a stack of recurrent units representing different components of the time series, scalable to hundreds of thousands of nodes in a network using multi-head attention and importance-sampling on neighbors, able to represent underlying networks that change over time, and suitable for multivariate networked series with missing nodes and edges. We achieve state-of-the-art results on recent web-scale networked time series. We also show that the stack of recurrent units successfully decomposes time series into different seasonal and trend effects, and that the network attention aggregates and explains influence between nodes. Future work includes extending Radflow to other networked data types such as events over continuous time. One can explore a wide range of applications such as imputing geographic data or allocating network resources. It would also be interesting to investigate causal reasoning or counterfactual modeling with Radflow-like structures.

ACKNOWLEDGMENTS

This research is supported in part by the Australian Research Council Project DP180101985 and AOARD project 20IOA064. We thank NVIDIA for providing us with Titan V GPUs for experimentation.

REFERENCES

- [1] George Athanasopoulos, Rob Hyndman, Haiyan Song, and Doris C. Wu. 2011. The tourism forecasting competition. *International Journal of Forecasting* 27, 3 (2011), 822–844.
- [2] G. E. P. Box and G. M. Jenkins. 1970. *Time series analysis: Forecasting and control*. San Francisco: Holden-Day.
- [3] Robert Goodell Brown. 1959. *Statistical forecasting for inventory control*. McGraw/Hill.
- [4] Deng Cai and Wai Lam. 2020. Graph Transformer for Graph-to-Sequence Learning. In *AAAI*. 7464–7471.
- [5] Cristian Consonni, David Laniado, and Alberto Montresor. 2019. WikiLinkGraphs: A complete, longitudinal and multi-language dataset of the Wikipedia link networks. In *Proceedings of the International AAAI Conference on Web and Social Media*, Vol. 13. 598–607.
- [6] Vasant Dhar, Tomer Geva, Gal Oestreicher-Singer, and Arun Sundararajan. 2014. Prediction in economic networks. *Information Systems Research* 25, 2 (2014), 264–284.
- [7] Aditya Grover and Jure Leskovec. 2016. node2vec: Scalable feature learning for networks. In *Proceedings of the 22nd ACM SIGKDD international conference on Knowledge discovery and data mining*. 855–864.
- [8] Will Hamilton, Zhitao Ying, and Jure Leskovec. 2017. Inductive representation learning on large graphs. In *Advances in neural information processing systems*. 1024–1034.
- [9] Dan Hendrycks and Kevin Gimpel. 2016. Gaussian Error Linear Units (GELUs). *arXiv: Learning* (2016).
- [10] CC Holt. 1957. Forecasting seasonals and trends by exponentially weighted averages (O.N.R. Memorandum No. 52). *Carnegie Institute of Technology* (1957).
- [11] R.J. Hyndman and G. Athanasopoulos. 2018. *Forecasting: principles and practice* (2nd editio ed.). OTexts: Melbourne, Australia. OTexts.com/fpp2
- [12] Mirko Kämpf, Eric Tessenow, Dror Y Kenett, and Jan W Kantelhardt. 2015. The detection of emerging trends using Wikipedia traffic data and context networks. *PLoS one* 10, 12 (2015), e0141892.
- [13] Diederik P. Kingma and Jimmy Ba. 2015. Adam: A Method for Stochastic Optimization. In *International Conference on Learning Representations*.
- [14] Thomas N. Kipf and Max Welling. 2017. Semi-Supervised Classification with Graph Convolutional Networks. In *International Conference on Learning Representations (ICLR)*.
- [15] Ilya Loshchilov and Frank Hutter. 2019. Decoupled Weight Decay Regularization. In *International Conference on Learning Representations*.
- [16] Spyros Makridakis and Michele Hibon. 2000. The M3-Competition: results, conclusions and implications. *International Journal of Forecasting* 16, 4 (2000), 451–476.
- [17] Spyros Makridakis, Evangelos Spiliotis, and Vassilios Assimakopoulos. 2018. The M4 Competition: Results, findings, conclusion and way forward. *International Journal of Forecasting* 34, 4 (2018), 802–808.
- [18] Franco Manessi, Alessandro Rozza, and Mario Manzo. 2020. Dynamic Graph Convolutional Networks. *Pattern Recognit.* 97 (2020).
- [19] Swapnil Mishra, Marian-Andrei Rizoïu, and Lexing Xie. 2016. Feature driven and point process approaches for popularity prediction. In *Proceedings of the 25th ACM international conference on information and knowledge management*. 1069–1078.
- [20] Gal Oestreicher-Singer, Barak Libai, Liron Sivan, Eyal Carmi, and Ohad Yassin. 2013. The network value of products. *Journal of Marketing* 77, 3 (2013), 1–14.
- [21] Boris N. Oreshkin, Dmitri Carpov, Nicolas Chapados, and Yoshua Bengio. 2020. N-BEATS: Neural basis expansion analysis for interpretable time series forecasting. In *International Conference on Learning Representations*.
- [22] Aldo Pareja, Giacomo Domeniconi, Jian Jhen Chen, Tengfei Ma, Toyotaro Suzumura, Hiroki Kanezashi, Tim Kaler, and Charles E. Leiserson. 2019. EvolveGCN: Evolving Graph Convolutional Networks for Dynamic Graphs. *ArXiv abs/1902.10191* (2019).
- [23] Adam Paszke, Sam Gross, Soumith Chintala, Gregory Chanan, Edward Yang, Zachary DeVito, Zeming Lin, Alban Desmaison, Luca Antiga, and Adam Lerer. 2017. Automatic Differentiation in PyTorch. In *NIPS Autodiff Workshop*.
- [24] Bryan Perozzi, Rami Al-Rfou, and Steven Skiena. 2014. DeepWalk: Online Learning of Social Representations. In *Proceedings of the 20th ACM SIGKDD International Conference on Knowledge Discovery and Data Mining (KDD '14)*. Association for Computing Machinery, New York, NY, USA, 701–710.
- [25] N. Petluri and E. Al-Masri. 2018. Web Traffic Prediction of Wikipedia Pages. In *2018 IEEE International Conference on Big Data (Big Data)*. 5427–5429.
- [26] Benedek Rozemberczki, Carl Allen, and Rik Sarkar. 2019. Multi-scale Attributed Node Embedding. *arXiv:cs.LG/1909.13021*
- [27] Aravind Sankar, Yanhong Wu, Liang Gou, Wei Zhang, and Hao Yang. 2020. DySAT: Deep Neural Representation Learning on Dynamic Graphs via Self-Attention Networks. In *Proceedings of the 13th International Conference on Web Search and Data Mining*. 519–527.
- [28] Minjeong Shin, Alasdair Tran, Siqi Wu, Alexander Mathews, Rong Wang, Georgiana Lyall, and Lexing Xie. 2021. AttentionFlow: Visualising Influence in Networks of Time Series. In *The 14th International Conference on Web Search and Data Mining, Demo (WSDM '21)*.
- [29] Jessica Su, Aneesh Sharma, and Sharad Goel. 2016. The effect of recommendations on network structure. In *Proceedings of the 25th international conference on World Wide Web*. 1157–1167.
- [30] Gabor Szabo and Bernardo A Huberman. 2010. Predicting the popularity of online content. *Commun. ACM* 53, 8 (2010), 80–88.
- [31] Alasdair Tran, Alexander Mathews, Cheng Soon Ong, and Lexing Xie. 2021. Radflow: A Recurrent, Aggregated, and Decomposable Model for Networks of Time Series – Supplementary Materials. <https://github.com/alsadairtran/radflow>.
- [32] Rakshit Trivedi, Hanjun Dai, Yichen Wang, and Le Song. 2017. Know-evolve: deep temporal reasoning for dynamic knowledge graphs. In *Proceedings of the 34th International Conference on Machine Learning-Volume 70*. 3462–3471.
- [33] Rakshit Trivedi, Mehrdad Farajtabar, Prasenjeet Biswal, and Hongyuan Zha. 2019. Dyrep: Learning representations over dynamic graphs. In *International Conference on Learning Representations*.
- [34] Ashish Vaswani, Noam Shazeer, Niki Parmar, Jakob Uszkoreit, Llion Jones, Aidan N. Gomez, Lukasz Kaiser, and Illia Polosukhin. 2017. Attention is All you Need. *ArXiv abs/1706.03762* (2017).
- [35] Petar Veličković, Guillem Cucurull, Arantxa Casanova, Adriana Romero, Pietro Liò, and Yoshua Bengio. 2018. Graph Attention Networks. In *International Conference on Learning Representations*.
- [36] Peter R Winters. 1960. Forecasting sales by exponentially weighted moving averages. *Management science* 6, 3 (1960), 324–342.
- [37] Neo Z. Wu, Bradley A. Green, Xue Ben, and Shawn O'Banion. 2020. Deep Transformer Models for Time Series Forecasting: The Influenza Prevalence Case. *ArXiv abs/2001.08317* (2020).
- [38] Siqi Wu, Marian-Andrei Rizoïu, and Lexing Xie. 2019. Estimating Attention Flow in Online Video Networks. *Proc. ACM Hum.-Comput. Interact.* 3, CSCW, Article 183 (Nov. 2019), 25 pages. <https://doi.org/10.1145/3359285>
- [39] Kun Xu, Lingfei Wu, Zhiguo Wang, Yansong Feng, Michael Witbrock, and Vadim Sheinin. 2018. Graph2seq: Graph to sequence learning with attention-based neural networks. *arXiv preprint arXiv:1804.00823* (2018).
- [40] Ling Zhao, Yujiao Song, Chao Zhang, Yu Liu, Pu Wang, Tao Lin, Min Deng, and Haifeng Li. 2019. T-GCN: A Temporal Graph Convolutional Network for Traffic Prediction. *IEEE Transactions on Intelligent Transportation Systems* (2019), 1–11.
- [41] Kai Zhu, Dylan Walker, and Lev Muchnik. 2020. Content Growth and Attention Contagion in Information Networks: Addressing Information Poverty on Wikipedia. *Information Systems Research* (2020).
- [42] Lingxue Zhu and Nikolay Laptev. 2017. Deep and Confident Prediction for Time Series at Uber. *2017 IEEE International Conference on Data Mining Workshops (ICDMW)* (2017), 103–110.

A ON LOS-LOOP AND SZ-TAXI

We first discuss some peculiarities found in SZ-TAXI. Fig. 10 shows that SZ-TAXI is noisier than LOS-LOOP, which explains SZ-TAXI’s worse SMAPE scores across all model variants in Table 4. We also see a drop in the median speed during the training period of SZ-TAXI (Fig. 10 bottom). This leads to a small positive bias in the final predictions of Radflow during the test period (Fig. 11). Such bias is not observed in the copying baseline.

Upon closer inspection of the ground-truth measurements in SZ-TAXI’s test period, we find that 28% of the data points are exactly zero. Many of these zero measurements happen consecutively. Recall that the SMAPE metric is sensitive to zero values. In particular, if the ground-truth value is zero and the predicted value is non-zero, we obtain the maximum SMAPE of 200. Meanwhile, both RMSE and MAE do not suffer from this problem at zero. This explains why in Table 4, the Radflow variant gets a relatively bad SMAPE score but a good RMSE and MAE. To confirm this effect, Table 7 presents metrics both on all test measurements and on only non-zero test measurements. We see that when we exclude the zero measurements, SMAPE correlates better with RMSE and MAE, and Radflow now outperforms the copying baseline.

Finally from Table 8, we see that on both datasets, our Radflow-NoNetwork have statistically similar performance to T-GCN. Our full Radflow outperforms T-GCN in LOS-LOOP while it has comparable performance to T-GCN in SZ-TAXI.

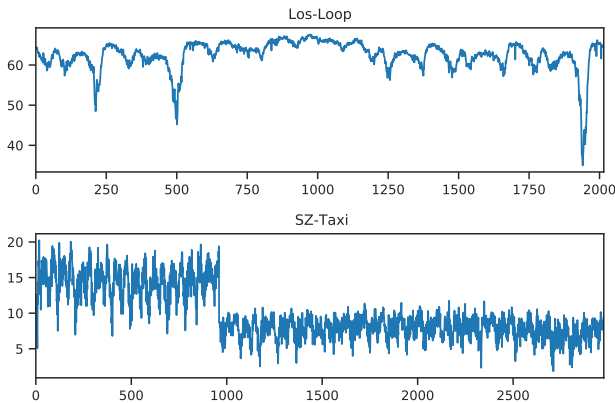


Figure 10: The median of the ground-truth time series across all samples in LOS-LOOP (top) and SZ-TAXI (bottom).

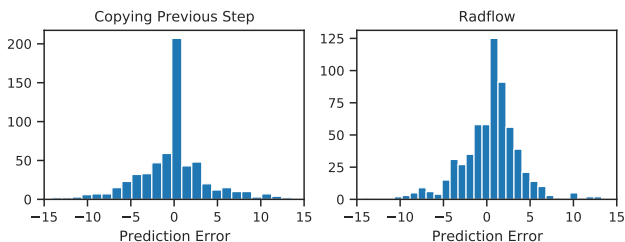


Figure 11: Prediction errors on SZ-TAXI.

Table 7: FORECAST performance on SZ-TAXI. We report mean SMAPE-4, RMSE-4, and MAE-4. We consider both the setting where we use all test measurements and the one where we only use non-zero measurements.

	All Measurements			Non-zero Measurements		
	SMAPE	RMSE	MAE	SMAPE	RMSE	MAE
(1) Copying Previous Step	45.8	4.32	2.81	49.6	4.92	3.68
(8) Radflow-NoNetwork	80.2	3.99	3.06	32.7	3.99	3.03
(9) T-GCN [40]	80.5	6.27	3.52	33.1	4.98	3.15
(15) Radflow	77.5	3.36	2.51	29.0	3.40	2.52

Table 8: Selected p-values from the dependent t-test for paired samples on LOS-LOOP and SZ-TAXI. The models are numbered according to Sec 6.1. We only show model pairs where the p-value is at least 0.001. For SZ-TAXI, we distinguish between the metrics computed on all test measurements (SZ-TAXI-A) and on only non-zero measurements (SZ-TAXI-N).

Dataset	Group 1		Group 2		p-value
	Model	SMAPE	Model	SMAPE	
LOS-LOOP	(1) Copying Previous Step	3.92	(9) T-GCN	3.97	0.674
LOS-LOOP	(8) Radflow-NoNetwork	3.60	(9) T-GCN	3.97	0.002
SZ-TAXI-A	(8) Radflow-NoNetwork	80.2	(9) T-GCN	80.5	0.949
SZ-TAXI-A	(9) T-GCN	80.5	(15) Radflow	77.5	0.509
SZ-TAXI-N	(8) Radflow-NoNetwork	32.7	(9) T-GCN	33.1	0.874
SZ-TAXI-N	(9) T-GCN	33.1	(15) Radflow	29.0	0.090

B FURTHER DISCUSSION ON RADFLOW

We start by discussing possible interpretations of the attention scores in Radflow. We then present results on how the performance is affected by the topic category and the popularity of a page in WIKITRAFFIC. Finally we provide further hyperparameters and statistical significance tests for experiments on both VEVO MUSIC and WIKITRAFFIC.

B.1 Attention scores

Analyzing attention scores can provide insights into both the data and the model. To this end, we show how two types of information are captured by the scores—the flow of traffic from neighboring pages and the time series correlation.

B.1.1 Spikes from neighbors. Fig. 12 shows view counts of Andy Gavin’s (a video game programmer) Wikipedia page and three linked articles with shading indicating attention scores, i.e. λ in Eq. (21). The scores are extracted from Radflow in the IMPUTATION setting. During the forecast period, details of a new video game *Crash Bandicoot 4* were released, leading to a spike in traffic on Andy Gavin’s page (the designer of the original *Crash Bandicoot*). Linked articles, e.g., *Naughty Dog* (the company Gavin co-founded), exhibit similar spikes to which substantial attention is applied. This example supports the intuition that network attention is important when an exogenous event causes traffic on neighboring nodes to change rapidly.

B.1.2 Time series correlation. To further investigate what kind of information the attention scores capture, Fig. 13 presents a density

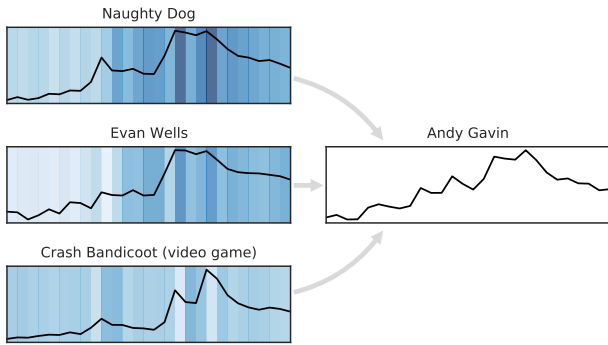


Figure 12: An example where Radflow attends to three neighbors as it forecasts the traffic of *Andy Gavin* (video game programmer and entrepreneur). A darker blue corresponds to a higher attention on the corresponding day. The network effect is important when there is a surge in traffic.

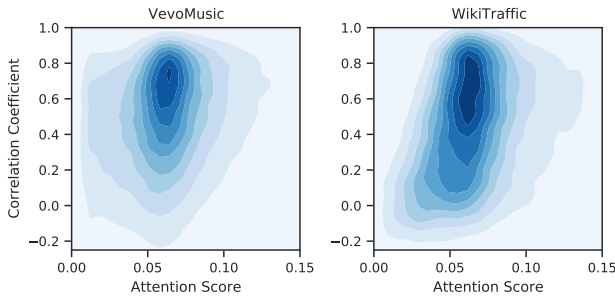


Figure 13: Density map of network attention scores (x-axis) and the correlation coefficient of a node with its neighbor (y-axis).

plot of correlation coefficients between the time series of an ego node and that of a neighbor, against the average attention score on the neighbor during the forecast period. On both *VEVOMUSIC* and *WIKITRAFFIC*, we observe that if two time series have a very low to negative correlation, the model will almost never output a high attention score. On *WIKITRAFFIC*, we also see that positively correlated time series rarely result in a low attention score.

B.2 Effect of Page Category and Popularity

On *WIKITRAFFIC*, we break our model’s performance down by both page category and page popularity, in order to see if these have any effect on the performance. From Fig. 14, we see that on both *Radflow-NoNetwork* and *Radflow*, there is no significant difference in the performance among the four test categories—Global Health, Global Warming, Programming, and Star Wars. Furthermore, the improvement in SMAPE from adding network information is consistent across these categories.

In contrast, the popularity of a page has a significant impact on how well the predictions are. From Fig. 15, we observe that there exists an optimal range of popularity where traffic is most

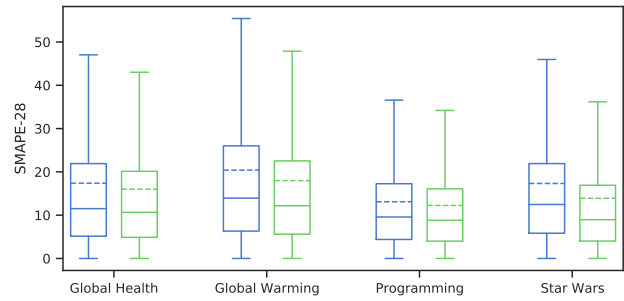


Figure 14: Performance broken down by categories in the test set of *WIKITRAFFIC* (univariate). The dashed lines indicate mean SMAPE-28. Blue boxplots correspond to *Radflow-NoNetwork*, while green boxplots correspond to *Radflow* with one-hop aggregation. All categories benefit from the network information.

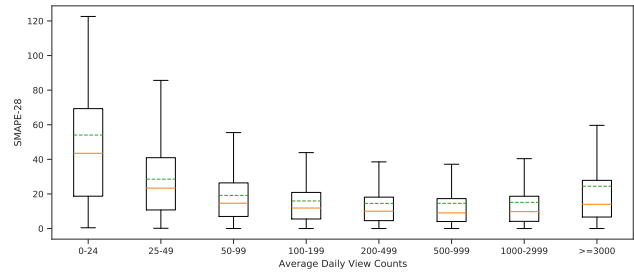


Figure 15: *Radflow-NoNetwork*’s performance on *WIKITRAFFIC* (univariate), broken down by the popularity of a page. The dashed lines indicate mean SMAPE-28. There exists an optimal range of popularity where traffic is the most predictable, resulting in a low SMAPE.

predictable. Our model is best at forecasting pages that have between 200 and 1,000 daily visits. Pages with fewer than 50 daily visits are fairly difficult to forecast. This matches the observation we made on *SZ-TAXI*, where it is also difficult to forecast the low traffic speeds. More interestingly, our model’s performance also drops slightly with very popular pages (those with more than 1,000 daily views). This could be due the traffic of these popular pages being driven mostly by events external to the network.

B.3 Hyperparameters and Significance Tests

This final section provides further details on the hyperparameters and statistical significance tests. In the main paper, Table 2 shows the hyperparameters of our two key models, *Radflow-NoNetwork* and *Radflow*. Tables 9 and 10 provide hyperparameters of the remaining model variants. Finally Table 11 contains the p-values from the dependent t-test for paired samples on *VEVOMUSIC* and *WIKITRAFFIC*. We note that if two models differ by more than one digit in the third significant figure, it is sufficient to conclude that the difference is statistically significant in these datasets (i.e. p-value < 0.05).

Table 9: Hyperparameters of pure time series models. Rows are numbered according to Sec 6.1. All model variants use 8 layers with a dropout of 0.1. For each dataset, we calibrate the hidden size so that the number of parameters between all models are within 5% of each other. Note that the N-BEATS model for WIKITRAFFIC (bivariate) consists of two separate models, one predicting the desktop traffic and the other predicting the combined mobile/app traffic. Each of these two models contains 829,760 parameters.

Dataset	Model	Hidden Size	Parameters
VEVOMUSIC	(6) LSTM	164	1,625,078
	(7) N-BEATS	192	1,630,480
	(8) Radflow-NoNetwork	128	1,589,762
WIKITRAFFIC (univariate)	(6) LSTM	164	1,625,078
	(7) N-BEATS	176	1,610,176
	(8) Radflow-NoNetwork	128	1,589,762
WIKITRAFFIC (bivariate)	(6) LSTM	164	1,625,900
	(7) N-BEATS	120	1,659,520
	(8) Radflow-NoNetwork	128	1,590,020
LOS-LOOP	(8) Radflow-NoNetwork	73	260,758
	(9) T-GCN [40]	292	261,060
SZ-TAXI	(8) Radflow-NoNetwork	73	260,758
	(9) T-GCN [40]	294	262,252

Table 10: Hyperparameters of time series models with network information. Rows are numbered according to Sec 6.1. All model variants use 8 layers with a dropout of 0.1. For each dataset, we calibrate the hidden size so that the number of parameters between all models are within 5% of each other. Some model variants were not evaluated under the two-hop setting and are indicated with a hyphen.

Dataset	Model	One Hop		Two Hops	
		Hidden Size	Parameters	Hidden Size	Parameters
VEVOMUSIC	(11) LSTM-MeanPooling	160	1,598,562	160	1,650,082
	(12) Radflow-MeanPooling	120	1,632,604	120	1,632,604
	(13) Radflow-GraphSage	118	1,606,928	118	1,634,894
	(14) Radflow-GAT	120	1,647,364	120	1,662,124
	(15) Radflow	116	1,608,112	112	1,576,180
	(16) Radflow (\mathbf{h} as embeddings)	124	1,586,088	-	-
	(17) Radflow (\mathbf{p} as embeddings)	124	1,586,088	-	-
	(18) Radflow (\mathbf{q} as embeddings)	124	1,586,088	-	-
	(19) Radflow ($[\mathbf{h}; \mathbf{p}]$ as embeddings)	116	1,632,588	-	-
	(20) Radflow ($[\mathbf{h}; \mathbf{p}; \mathbf{q}]$)	104	1,639,564	-	-
	(21) Radflow (no final projection)	116	1,608,112	-	-
	(22) Radflow (one head)	116	1,608,112	-	-
WIKITRAFFIC (bivariate)	(11) LSTM-MeanPooling	160	1,599,364	160	1,650,884
	(12) Radflow-MeanPooling	120	1,632,968	120	1,632,968
	(13) Radflow-GraphSage	118	1,607,286	118	1,635,252
	(14) Radflow-GAT	120	1,647,728	120	1,662,488
	(15) Radflow	116	1,608,464	112	1,576,520
LOS-LOOP	(15) Radflow	64	260,036	-	-
SZ-TAXI	(15) Radflow	64	260,036	-	-

Table 11: Selected p-values from the dependent t-test for paired samples on VEVO MUSIC and WIKITRAFFIC. Models are numbered according to Sec 6.1. We only show pairs where the p-value is at least 0.001. We observe that if two models differ by more than one digit in the third significant figure, their difference is statistically significant in these datasets ($p < 0.05$).

	Group 1			Group 2			p-value	
	Model	Hops	SMAPE	Model	Hops	SMAPE		
VEVO MUSIC	(6) LSTM	0H	8.68	(7) N-BEATS	0H	8.64	0.006	
VEVO MUSIC (static)	FORECAST	(12) Radflow-MeanPooling	1H	8.34	(15) Radflow	1H	8.33	0.171
		(13) Radflow-GraphSage	1H	8.39	(13) Radflow-GraphSage	2H	8.37	0.036
		(13) Radflow-GraphSage	1H	8.39	(15) Radflow	2H	8.39	0.938
		(14) Radflow-GAT	1H	8.52	(14) Radflow-GAT	2H	8.50	0.018
		(13) Radflow-GraphSage	2H	8.37	(15) Radflow	2H	8.39	0.014
	IMPUTATION	(11) LSTM-MeanPooling	1H	8.14	(11) LSTM-MeanPooling	2H	8.13	0.117
		(12) Radflow-MeanPooling	1H	7.82	(12) Radflow-MeanPooling	2H	7.81	0.376
		(15) Radflow	1H	7.67	(13) Radflow-GraphSage	2H	7.64	0.001
		(13) Radflow-GraphSage	2H	7.64	(15) Radflow	2H	7.63	0.017
VEVO MUSIC (dynamic)	FORECAST	(12) Radflow-MeanPooling	1H	8.42	(13) Radflow-GraphSage	1H	8.43	0.618
		(12) Radflow-MeanPooling	1H	8.42	(14) Radflow-GAT	1H	8.43	0.586
		(13) Radflow-GraphSage	1H	8.43	(14) Radflow-GAT	1H	8.43	0.987
		(15) Radflow	1H	8.37	(14) Radflow-GAT	2H	8.39	0.001
		(13) Radflow-GraphSage	2H	8.46	(15) Radflow	2H	8.45	0.064
	IMPUTATION	(11) LSTM-MeanPooling	1H	7.91	(11) LSTM-MeanPooling	2H	7.90	0.702
		(13) Radflow-GraphSage	1H	7.46	(14) Radflow-GAT	1H	7.44	0.007
		(13) Radflow-GraphSage	2H	7.27	(14) Radflow-GAT	2H	7.28	0.091
		(13) Radflow-GraphSage	2H	7.27	(15) Radflow	2H	7.27	0.871
		(14) Radflow-GAT	2H	7.28	(15) Radflow	2H	7.27	0.110
WIKITRAFFIC (univariate)	FORECAST	(6) LSTM	0H	16.6	(7) N-BEATS	0H	16.6	0.471
		(6) LSTM	0H	16.6	(11) LSTM-MeanPooling	2H	16.7	0.002
		(6) LSTM	0H	16.6	(13) Radflow-GraphSage	2H	16.7	0.067
		(7) N-BEATS	0H	16.6	(12) Radflow-MeanPooling	2H	16.5	0.002
		(7) N-BEATS	0H	16.6	(13) Radflow-GraphSage	2H	16.7	0.016
		(8) Radflow-NoNetwork	0H	16.1	(14) Radflow-GAT	1H	16.2	0.019
		(8) Radflow-NoNetwork	0H	16.1	(15) Radflow	1H	16.2	0.027
		(12) Radflow-MeanPooling	1H	16.5	(12) Radflow-MeanPooling	2H	16.5	0.105
		(14) Radflow-GAT	1H	16.2	(15) Radflow	1H	16.2	0.948
		(11) LSTM-MeanPooling	2H	16.7	(13) Radflow-GraphSage	2H	16.7	0.139
	(14) Radflow-GAT	2H	16.0	(15) Radflow	2H	16.0	0.934	
	IMPUTATION	(12) Radflow-MeanPooling	1H	15.1	(14) Radflow-GAT	1H	15.1	0.844
		(12) Radflow-MeanPooling	1H	15.1	(13) Radflow-GraphSage	2H	15.0	0.001
		(14) Radflow-GAT	1H	15.1	(12) Radflow-MeanPooling	2H	15.1	0.001
		(14) Radflow-GAT	1H	15.1	(13) Radflow-GraphSage	2H	15.0	0.001
(11) LSTM-MeanPooling		2H	15.2	(12) Radflow-MeanPooling	2H	15.1	0.098	
WIKITRAFFIC (bivariate)	FORECAST	(7) N-BEATS	0H	20.3	(11) LSTM-MeanPooling	1H	20.2	0.013
		(7) N-BEATS	0H	20.3	(12) Radflow-MeanPooling	2H	20.2	0.015
		(8) Radflow-NoNetwork	0H	19.4	(13) Radflow-GraphSage	1H	19.4	0.112
		(11) LSTM-MeanPooling	1H	20.2	(12) Radflow-MeanPooling	2H	20.2	0.680
		(15) Radflow	1H	19.9	(11) LSTM-MeanPooling	2H	19.9	0.380
		(15) Radflow	1H	19.9	(13) Radflow-GraphSage	2H	19.9	0.172
		(11) LSTM-MeanPooling	2H	19.9	(13) Radflow-GraphSage	2H	19.9	0.104
		(14) Radflow-GAT	2H	19.7	(15) Radflow	2H	19.6	0.487
	IMPUTATION	(12) Radflow-MeanPooling	1H	18.5	(15) Radflow	2H	18.5	0.596
		(14) Radflow-GAT	1H	18.3	(15) Radflow	1H	18.3	0.825
		(14) Radflow-GAT	1H	18.3	(13) Radflow-GraphSage	2H	18.4	0.025
		(15) Radflow	1H	18.3	(13) Radflow-GraphSage	2H	18.4	0.019